IOPscience iopscience.iop.org

Home Search Collections Journals About Contact us My IOPscience

Dynamics of continuous-time quantum walks in restricted geometries

This article has been downloaded from IOPscience. Please scroll down to see the full text article.

2008 J. Phys. A: Math. Theor. 41 445301

(http://iopscience.iop.org/1751-8121/41/44/445301)

View the table of contents for this issue, or go to the journal homepage for more

Download details:
IP Address: 171.66.16.152
The article was downloaded on 03/06/2010 at 07:18

Please note that terms and conditions apply.

IOP PUBLISHING JOURNAL OF PHYSICS A: MATHEMATICAL AND THEORETICAL

J. Phys. A: Math. Theor. **41** (2008) 445301 (21pp) doi:10.1088/1751-8113/41/44/445301

Dynamics of continuous-time quantum walks in restricted geometries

E Agliari, A Blumen and O Mülken

Theoretische Polymerphysik, Universität Freiburg, Hermann-Herder-Str. 3, D-79104 Freiburg, Germany

Received 19 July 2008, in final form 4 September 2008
Published 7 October 2008
Online at stacks.iop.org/JPhysA/41/445301

Abstract

We study quantum transport on finite discrete structures and we model the process by means of continuous-time quantum walks. A direct and effective comparison between quantum and classical walks can be attained based on the average displacement of the walker as a function of time. Indeed, a fast growth of the average displacement can be advantageously exploited to build up efficient search algorithms. By means of analytical and numerical investigations, we show that the finiteness and the inhomogeneity of the substrate jointly weaken the quantum-walk performance. We further highlight the interplay between the quantum-walk dynamics and the underlying topology by studying the temporal evolution of the transfer probability distribution and the lower bound of long-time averages.

PACS numbers: 05.60.Gg, 71.35.−y, 05.60.Cd

(Some figures in this article are in colour only in the electronic version)

1. Introduction

Quantum walks (QWs) are attracting increasing attention in many research areas, ranging from solid-state physics to quantum computing [1]. In particular, QWs provide a model for quantum-mechanical transport processes on discrete structures; this includes, for instance, the coherent energy transfer of a qubit on an optical lattice [2–5]. The theoretical study of QWs is also encouraged by recent experimental implementations able to corroborate theoretical findings [6–8].

As in the classical random walk, quantum walks appear in a discrete [9] as well as in a continuous-time (CTQW) [10] form; these forms, however, cannot be simply related to each other [11]. Now, standard CTQWs, on which we focus, can be obtained by identifying the Hamiltonian of the system with the classical transfer matrix which is, in turn, directly related to the Laplacian of the underlying structure.

 © 2008 IOP Publishing Ltd Printed in the UK

Another feature which CTQWs share with classical random walks consists of the strong interplay between the dynamics properties displayed by the walk and the topology of the substrate [12–14]. However, the dependences turn out to be much more complex in the quantum-mechanical case: while the classical (simple) walk eventually loses memory of its starting site, the quantum walk exhibits, even in the asymptotic regime, transition probabilities which depend on the starting site. For this reason, often the parameters describing the transport are averaged over all initial sites, a procedure which allows a global characterization of the walk, while preserving its most important features.

One of the quantities affected by topology is the mean-square displacement of the walker up to time t. Classically, this quantity is monotonically increasing and depends (asymptotically) on time according to the power law $\langle r^2(t)\rangle \sim t^\beta$. The value of the 'diffusion exponent' β allows us to distinguish between normal ($\beta = 1$) and anomalous ($\beta \neq 1$) diffusion [15]. As for quantum transport, it is possible to introduce analogous exponents, characterizing the temporal spreading of a wave packet [16]. However, even when they take place over the same structure, quantum and classical walks can exhibit dramatically different behaviours. In particular, the quantum wave propagation on regular, infinite lattices is ballistic, i.e. the root-mean-square displacement is linear in time. Such a quadratic speed-up of the mean-square displacement is a well-known phenomenon when dealing with tight-binding electron waves on periodic lattices [9] and, from a computational point of view, it constitutes an important feature since it could be advantageously exploited in quantum search algorithms [17–19]. In the presence of disorder (either deterministic or stochastic) or finiteness, the sharp ballistic fronts are softened, a fact which may even lead to the localization of the quantum particle [20, 21]. It is therefore of both theoretical and practical interest to highlight how finiteness and inhomogeneity—often unavoidable in real systems—affect the particle's propagation. To this aim we analyse quantum transport on restricted geometries, where the restrictions arise from the (possibly joint) fractal dimension and finite extent of the substrate itself. By direct comparison with the classical case, we find that, on finite substrates, the advantage of CTQWs is at short times only. Moreover, the lack of translational invariance weakens the CTQW performance, i.e. in such situations the average displacement increases more slowly with time.

The finite discrete structures we consider and compare are the dual Sierpinski gasket (DSG), the Cayley tree (CT) *vide infra* section 4 and the square lattice with periodic boundary conditions, i.e. the square torus (ST). These constitute representative topologies, providing examples of fractals with loops, of trees and of regular structures. The dual Sierpinski gasket will be treated in more detail; for this structure the eigenvalue spectrum of the Laplacian matrix is known exactly, allowing for some analytical estimates. Indeed, not only random walks, but also many dynamical properties of connected structures themselves (such as the vibrational structures and the relaxation modes) depend on the spectrum of their Laplacian matrix [22]. However, for CTQWs the set of eigenvectors also matters, which often makes analytical investigations cumbersome.

It is worth underlining that focusing on discrete structures is not only suggested by solid-state applications: quantum computation is traditionally concerned with the manipulation of discrete systems. In particular, a discrete (and finite) state space makes the CTQW simulation by quantum computers, working with discrete registers, feasible [1, 23].

Our paper is structured as follows. After a brief summary of the main concepts and of the formulae concerning CTQWs in section 2, we describe the topology of the DSG in section 3. Then, in section 4, we study the quantum-mechanical transport over the above-mentioned structures, especially focusing on the average displacement and on the long-time averages. Finally, in section 5 we present our comments and conclusions. In the appendix,

we derive analytical results concerning the average chemical displacements of CTQWs over hypercubic lattices, special cases being chains and square lattices.

2. Continuous-time quantum walks on graphs

Mathematically, a graph is specified by the pair $\{V, E\}$ consisting of a nonempty, countable set of points V, joined pairwise by a set of links E. The cardinality of V provides the number $\mathcal{N}$ of sites making up the graph, i.e. its volume: $|V| = \mathcal{N}$. In the following, we focus mainly on finite graphs ($\mathcal{N} < \infty$) and we label each node with a lowercase letter $i \in V$.

From an algebraic point of view, a graph can be described by its adjacency matrix $\mathbf{A}$, whose elements are

$$A_{ij} = \begin{cases} 1, & \text{if} \quad (i, j) \in E, \\ 0, & \text{otherwise.} \end{cases}$$

The connectivity of a node i can be calculated as a sum of matrix elements $z_i = \sum_j A_{ij}$. The Laplacian operator is then defined as $\mathbf{L} = \mathbf{Z} - \mathbf{A}$, where $\mathbf{Z}$ is the diagonal matrix given by $Z_{ik} = z_i \delta_{ik}$.

The Laplacian matrix $\mathbf{L}$ is symmetric and non-negative definite and it can therefore generate a probability conserving Markov process and define a unitary process as well. Otherwise stated, the Laplacian operator can work both as a classical transfer operator and as a tight-binding Hamiltonian of a quantum transport process [24, 25].

Indeed, the classical continuous-time random walk (CTRW) is described by the following Master equation [26]:

$$\frac{\mathrm{d}}{\mathrm{d}t} p_{k,j}(t) = \sum_{l=1}^{\mathcal{N}} T_{kl}\, p_{l,j}(t), \tag{1}$$

where $p_{k,j}(t)$ is the conditional probability that the walker is on node k when it started from node j at time 0. If the walk is symmetric with a site-independent transmission rate γ, then the transfer matrix $\mathbf{T}$ is simply related to the Laplacian operator through $\mathbf{T} = -\gamma \mathbf{L}$.

Now the CTQW, the quantum-mechanical counterpart of the CTRW, is introduced by identifying the Hamiltonian of the system with the classical transfer matrix, $\mathbf{H} = -\mathbf{T}$ [10, 13, 24] (in the following we will set $\hbar \equiv 1$). The set of states $|j\rangle$, representing the walker localized at the node j, spans the whole accessible Hilbert space and also provides an orthonormal basis set. Therefore, the behaviour of the walker can be described by the transition amplitude $\alpha_{k,j}(t)$ from state $|j\rangle$ to state $|k\rangle$, which obeys the following Schrödinger equation:

$$\frac{\mathrm{d}}{\mathrm{d}t} \alpha_{k,j}(t) = -\mathrm{i} \sum_{l=1}^{\mathcal{N}} H_{kl} \alpha_{l,j}(t). \tag{2}$$

If at the initial time $t_0 = 0$ only the state $|j\rangle$ is populated, then the formal solution to equation (2) can be written as

$$\alpha_{k,j}(t) = \langle k| \exp(-\mathrm{i}\mathbf{H}t)|j\rangle, \tag{3}$$

whose squared magnitude provides the quantum-mechanical transition probability $\pi_{k,j}(t) \equiv |\alpha_{k,j}(t)|^2$. In general, it is convenient to introduce the orthonormal basis $|\psi_n\rangle, n \in [1, \mathcal{N}]$ which diagonalizes $\mathbf{T}$ (and, clearly, also $\mathbf{H}$); the correspondent set of eigenvalues is denoted by $\{\lambda_n\}_{n=1,\ldots,\mathcal{N}}$. Thus, we can write

$$\pi_{k,j}(t) = \left| \sum_{n=1}^{\mathcal{N}} \langle k|\, \mathrm{e}^{-\mathrm{i}\lambda_n t} |\psi_n\rangle\langle\psi_n|j\rangle \right|^2. \tag{4}$$

Despite the apparent similarity between equations (1) and (2), some important differences are worth being recalled.

First, the imaginary unit makes the time evolution operator $\mathbf{U}(t) = \exp(-\mathrm{i}\mathbf{H}t)$ unitary, which prevents the quantum-mechanical transition probability from having a definite limit as $t \to \infty$. On the other hand, a particle performing a CTRW is asymptotically equally likely to be found on any site of the structure: the classical $p_{k,j}(t)$ admit a stationary distribution which is independent of initial and final sites, $\lim_{t\to\infty} p_{k,j}(t) = 1/\mathcal{N}$. Hence, in order to compare classical long-time probabilities with quantum-mechanical ones, we rely on the long-time average (LTA) [27], defined in section 4.4.

Moreover, the normalization conditions for $p_{k,j}(t)$ and $\alpha_{k,j}(t)$ read $\sum_{k=1}^{\mathcal{N}} p_{k,j}(t) = 1$ and $\sum_{k=1}^{\mathcal{N}} |\alpha_{k,j}(t)|^2 = 1$.

2.1. Average displacement

The average displacement performed by a quantum walker until time t allows a straightforward comparison with the classical case; it is also more directly related to transport properties than the transfer probability $\pi_{k,j}(t)$: it constitutes the expectation value of the distance reached by the particle after a time t and its time dependence provides information on how fast the particle propagates over the substrate.

For CTQW (subscript q) starting at node j, we define the *average (chemical) displacement* $\langle r_j(t)\rangle_q$ performed until time t as

$$\langle r_j(t)\rangle_q = \sum_{k=1}^{\mathcal{N}} \ell(k, j)\pi_{k,j}(t), \tag{5}$$

where $\ell(k, j)$ is the chemical distance between the sites j and k, i.e. the length of the shortest path connecting j and k. We can average over all starting points to obtain

$$\overline{\langle r(t)\rangle}_q = \frac{1}{\mathcal{N}} \sum_{j=1}^{\mathcal{N}} \langle r_j(t)\rangle_q. \tag{6}$$

For fractals or hyperbranched structures it is more appropriate to use the chemical distance, rather than the Euclidean distance; for instance, the infinite CT (see section 4) cannot be embedded in any lattice of finite dimension. For classical diffusion, it is well known that the chemical and the Euclidean distances display analogous asymptotic laws for regular structures and for many deterministic fractals (e.g. the Sierpinski gasket) [15]; as discussed in the appendix, this still holds for CTQWs on arbitrary d-dimensional hypercubic lattices.

For classical (subscript c) regular diffusion (on infinite lattices) the average displacement $\langle r(t)\rangle_c$ depends on time t according to

$$\langle r(t)\rangle_c \sim t^{1/2}. \tag{7}$$

More generally, for scaling (fractal) structures we can define the so-called chemical diffusion exponent d_w^ℓ and get [15]:

$$\langle r(t)\rangle_c \sim t^{1/d_w^\ell}. \tag{8}$$

Finite systems require corrections to these laws: for them $\langle r(t)\rangle_c$ does not grow indefinitely, but it saturates to a maximum value r_c [28].

2.2. Return probability

As is well known, for a diffusive particle the probability to return to the starting point is topology sensitive and it can indeed be used to extract information about the underlying structure [26]. It is therefore interesting to compare the classical return probability $p_{k,k}(t)$ with the quantum-mechanical $\pi_{k,k}(t)$ (see also [29, 30]). One has

$$p_{k,k}(t) = \langle k|\exp(\mathbf{T}t)|k\rangle = \sum_{n=1}^{\mathcal{N}} |\langle k|\psi_n\rangle|^2 \exp(-\gamma t\lambda_n) \tag{9}$$

and

$$\pi_{k,k}(t) = \left|\alpha_{k,k}(t)\right|^2 = \left|\sum_{n=1}^{\mathcal{N}} |\langle k|\psi_n\rangle|^2 \exp(-\mathrm{i}\gamma t\lambda_n)\right|^2 . \tag{10}$$

In order to get a global information about the likelihood to be (return or stay) at the origin, independent of the starting site, we average over all sites of the graph, obtaining

$$\bar{p}(t) = \frac{1}{\mathcal{N}}\sum_{k=1}^{\mathcal{N}} p_{k,k}(t) = \frac{1}{\mathcal{N}}\sum_{n=1}^{\mathcal{N}} \mathrm{e}^{-\gamma\lambda_n t} \tag{11}$$

and

$$\bar{\pi}(t) = \frac{1}{\mathcal{N}}\sum_{k=1}^{\mathcal{N}} \pi_{k,k}(t) = \frac{1}{\mathcal{N}}\sum_{n,m=1}^{\mathcal{N}} \mathrm{e}^{-\mathrm{i}\gamma(\lambda_n-\lambda_m)t} \sum_{k=1}^{\mathcal{N}} |\langle k|\psi_n\rangle|^2\, |\langle k|\psi_m\rangle|^2 . \tag{12}$$

For finite substrates, the classical $\bar{p}(t)$ decays monotonically to the equipartition limit, and it only depends on the eigenvalues of $\mathbf{T}$. On the other hand, $\bar{\pi}(t)$ depends explicitly on the eigenvectors of $\mathbf{H}$ [29, 30]. By means of the Cauchy–Schwarz inequality we can obtain a lower bound for $\bar{\pi}(t)$ which does not depend on the eigenvectors [30, 31]:

$$\bar{\pi}(t) \geqslant \left|\frac{1}{\mathcal{N}}\sum_{k=1}^{\mathcal{N}} \alpha_{k,k}(t)\right| \equiv |\bar{\alpha}(t)|^2 = \frac{1}{\mathcal{N}^2}\sum_{m,n=1}^{\mathcal{N}} \mathrm{e}^{-\mathrm{i}\gamma(\lambda_n-\lambda_m)t}. \tag{13}$$

Note that equations (11) and (12) can serve as measures of the efficiency of the transport process performed by CTRW and CTQW, respectively. In fact, the faster $\bar{p}(t)$ decreases towards its asymptotic value, the more efficient the transport. Analogously, a more rapid decay of the envelope of $\bar{\pi}(t)$ (or of $|\bar{\alpha}(t)|^2$) implies a faster delocalization of the quantum walker over the graph. By the way, we recall that, for a large variety of graphs [30], the classical average return probability scales as $\bar{p}(t) \sim t^{-\mu}$, while the envelope of $|\bar{\alpha}(t)|^2$, namely env$[|\bar{\alpha}(t)|^2]$, scales like $t^{-2\mu}$, μ being a proper parameter related for fractals to the spectral density.

As can be inferred by comparing equations (11) and (12), for quantum transport processes the degeneracy of the eigenvalues plays an important role, as the differences between eigenvalues determine the temporal behaviour, while for classical transport the long-time behaviour is dominated by the smallest eigenvalue. Situations in which only a few, highly degenerate eigenvalues are present are related to slow CTQW dynamics, while when all eigenvalues are non-degenerate the transport turns out to be efficient [29, 30].

3. Dual Sierpinski gasket: topology and eigenvalue spectrum

Before turning to the dynamics of CTQW (and CTRW) on exemplary structures, which allow us to highlight the importance of inhomogeneities, some remarks on the spectra of the DSG are in order.

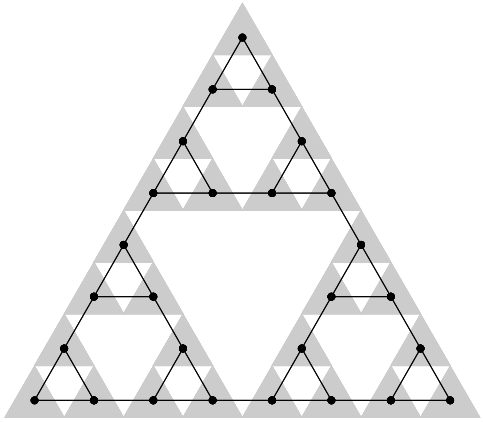

Figure 1. Dual transformation from Sierpinski gasket to dual Sierpinski gasket of generation $g = 3$.

The dual Sierpinski gasket is an exactly-decimable fractal which is directly related, through a dual transformation, to the Sierpinski gasket (SG). The DSG of generation g can be constructed by replacing each small triangle belonging to the SG with a node and by connecting such nodes whenever the relevant triangles share a vertex in the original gasket (see figure 1). It is straightforward to verify that the number of nodes at any given generation g is $\mathcal{N} = 3^g$.

The dual transformation does not conserve the coordination number of the inner nodes (which decreases from 4 to 3), but it does conserve the fractal dimension d_f and the spectral dimension $\tilde{d}$, which are therefore the same as for the original Sierpinski gasket $d_f = \ln 3/\ln 2 = 1.58496\ldots$ and $\tilde{d} = 2\ln 3/\ln 5 = 1.36521\ldots$.

As mentioned above, the knowledge of the eigenvalue spectrum is sufficient for the calculation of several interesting quantities concerning the dynamics of CTQWs. In general, any (finite) Hamiltonian **H** can be (at least numerically) diagonalized in order to obtain its spectrum. However, as the size of **H** gets large, the procedure gets to be time consuming and the precise numerical diagonalization may not be easy to perform. Remarkably, the eigenvalue spectrum of the DSG Laplacian matrix can be determined at any generation through the following iterative procedure; for more details we refer to [34, 35]: at any given generation g the spectrum includes the non-degenerate eigenvalue $\lambda_{\mathcal{N}} = 0$, the eigenvalue 3 with degeneracy $(3^{g-1}+3)/2$ and the eigenvalue 5 with degeneracy $(3^{g-1}-1)/2$. Moreover, given the eigenvalue spectrum at generation $g-1$, each non-vanishing eigenvalue λ_{g-1} corresponds to two new eigenvalues $\lambda_g^{\pm}$ according to

$$\lambda_g^{\pm} = \frac{5 \pm \sqrt{25 - 4\lambda_{g-1}}}{2}; \tag{14}$$

both λ_g^+ and λ_g^- inherit the degeneracy of λ_{g-1}. The eigenvalue spectra is therefore bounded in $[0, 5]$. As explained in [34], at any generation g, we can calculate the degeneracy of each distinct eigenvalue: apart from $\lambda_{\mathcal{N}}$ whose degeneracy is 1, there are 2^r distinct eigenvalues, each with degeneracy $(3^{g-r-1}+3)/2$, being $r = 0, 1, \ldots, g-1$, and 2^r distinct eigenvalues, each with degeneracy $(3^{g-r-1}-1)/2$, being $r = 0, 1, \ldots, g-2$. As can be easily verified, the degeneracies sum up to $\mathcal{N} = 3^g$. Finally, note that the distribution of eigenvalues and their degeneracies are non-uniform and that the spectrum is multifractal [34].

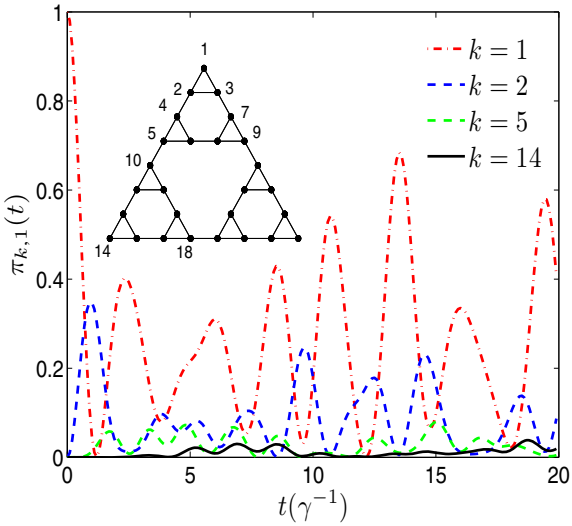

Figure 2. Exact probability $\pi_{k,1}(t)$ for the CTQW starting from the apex (site $j = 1$) to reach sites $k = 1, 2, 5$ and 14. The k-sites are the left corners at generations $g = 0, 1, 2$ and 3, respectively.

4. CTQWs on restricted geometries

4.1. Transfer probability

Results for the exact transition probability distribution $\pi_{k,j}(t)$ for STs and CTs have already been given in [13, 31, 32], where it was shown that $\pi_{k,j}(t)$ depends significantly on the starting node. The results for ultrametric structures are given in [33].

It is worth recalling here that the Cayley tree (CT) can be built by starting from one node (root) connected to z nodes, which constitute the first shell. Each node of the first shell is then connected to $z - 1$ new nodes, which constitute the second shell and so forth, iteratively. Therefore, the Mth shell contains $z(z-1)^{M-1}$ nodes which are at a chemical distance M from the root. Thus, the CT is a z-regular loop-free graph. The number of sites in a CT of M shells is $\mathcal{N}_M = [z(z-1)^M - 2]/(z-2)$, hence the correlated fractal dimension $\log(\mathcal{N}_M)/\log(M)$ goes to infinity for $M \to \infty$, precluding the possibility of embedding very large CT in any previously specified Euclidean lattice. In the following we focus on finite 3-Cayley trees, which means that z is fixed and equal to three for any internal site of the graph; furthermore, the number of shells (also called generation) is finite (and therefore also the number of nodes is itself finite).

In figure 2 we show our results for a DSG of generation $g = 3$ and we focus on the set of pairs given by $(v_n, 1)$, where v_n denotes any of the two corners of the gasket of the nth generation, with $n \leqslant g$ (i.e., according to the labelling of figure 2, $v_0 = 1, v_1 = 2$, $v_2 = 5, v_3 = 14$). Now, due to the symmetry the DSG is endowed with, for CTQWs starting from a given vertex, say the apex, the left and right corners are equivalent. As expected, $\pi_{k,j}(t)$ does not converge to any definite value, but it displays oscillations whose amplitudes and average values get smaller as the distance between the sites 1 and v_n increases. This suggests, at least when starting from a main vertex, that the CTQW stays mainly localized at the origin and its neighbourhood.

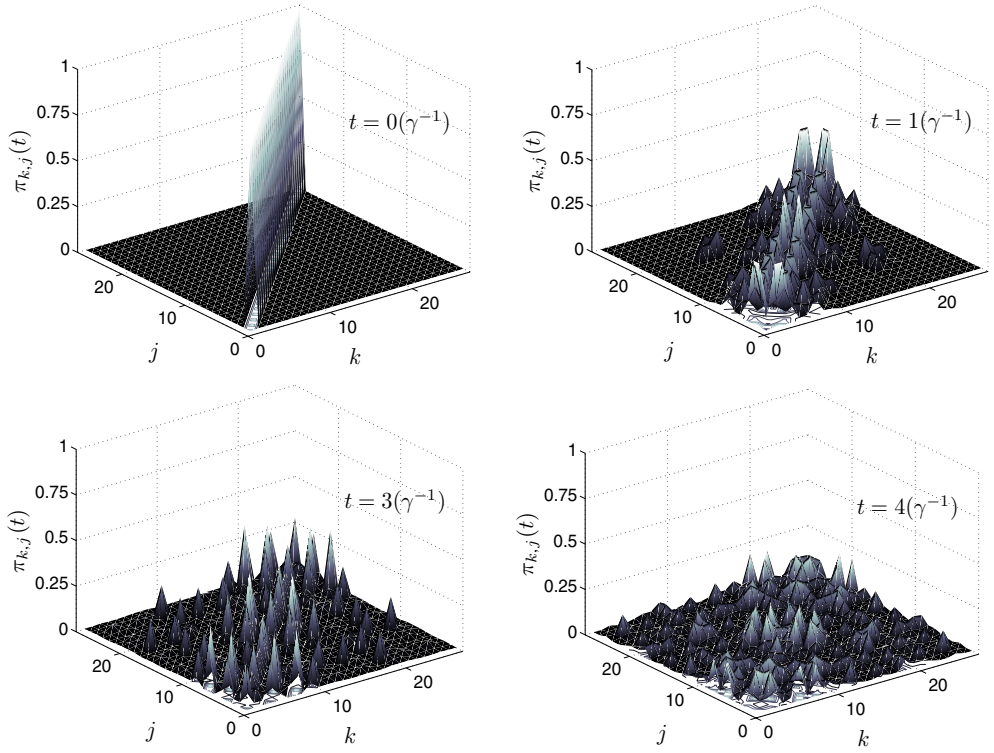

Figure 3. Snapshots of the transition probability $\pi_{k,j}(t)$ at different times $t = 0, 1, 3, 4$ (in units of γ^{-1}) for the dual Sierpinski gasket of generation $g = 3$ ($\mathcal{N} = 27$).

We corroborate this by looking at the temporal evolution of $\pi_{k,j}(t)$ for the DSG and by comparing it to the $\pi_{k,j}(t)$ pertaining to the CT and the ST of comparable size $\mathcal{N}$. Figures 3–5 show 3D pictures of $\pi_{k,j}(t)$ at different moments t (belonging to the short-time regime). On both the x and the y-axes, k and j label the nodes of the graph in such a way that at the point (k, j) on the xy plane the value of $\pi_{k,j}(t)$ is presented. At the initial time $t = 0$, the transition probability $\pi_{k,j}(t)$ is non-vanishing only on the diagonal, i.e. one has $\pi_{k,j}(0) = \delta_{k,j}$; at later times, $\pi_{k,j}(t)$ spreads out non-uniformly, according to the topology of the substrate. In particular, for the DSG (figure 3), a large fraction of $\pi_{k,j}(t)$ stays in a region connected by bonds to the initial nodes; several peaks can be distinguished, whose heights decrease as the chemical distance between the pertaining sites gets larger. For the CT, the pattern representing $\pi_{k,j}(t)$ is even more inhomogeneous; as can be inferred from figure 4, a quantum particle on the CT is located with very high probability on its initial node (except when starting from the central node) and, for the timescale considered, it is very unlikely to reach nodes outside its starting branch. On the other hand, for the ST (figure 5) we note that the spread of $\pi_{k,j}(t)$ is rapid and regular: apart from possibly partial revival phenomena (see for example the snapshot for $t = 3\gamma^{-1}$), the pattern for $\pi_{k,j}(t)$ exhibits very low peaks.

Indeed, peaks in $\pi_{k,j}(t)$ are a consequence of the constructive interference stemming from reflections at peripheral sites or (in the case of the torus) from the superposition of travelling waves which have crossed the whole (finite) graph.

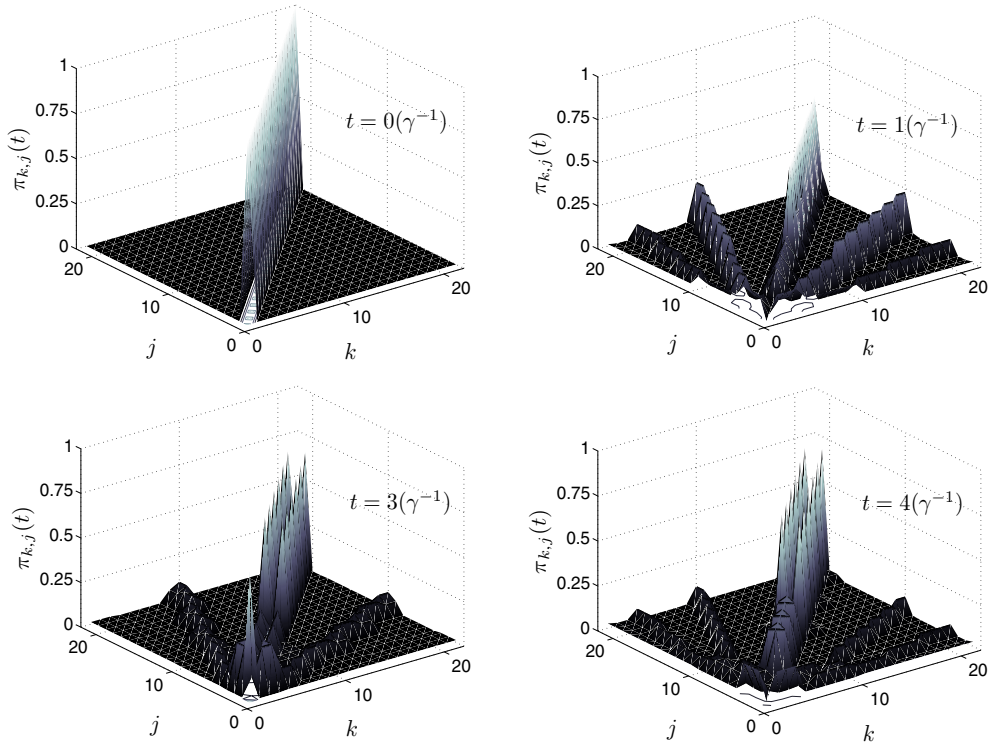

Figure 4. Snapshots of the transition probability $\pi_{k,j}(t)$ at different times $t = 0, 1, 3, 4$ for a Cayley tree of generation $g = 3$ ($\mathcal{N} = 3 \times 2^g - 2 = 22$); time is give in units of γ^{-1}. Note that the distribution is localized on special couples of nearest-neighbours sites and that also reflection effects appear.

Finally, figures 3–5 also highlight the symmetry characterizing the quantum transfer probability, namely that $\pi_{j,k}(t) = \pi_{k,j}(t)$, at all times. This can be derived directly from equation (3), recalling that **H** is itself symmetric and real. An analogous symmetry also characterizes the classical distribution $p_{j,k}(t)$ for all the cases analysed here.

4.2. Average displacement

The dynamics of quantum particles on non-regular structures has been investigated in several works meant to analyse the quantum dynamics of tight-binding electrons in quasicrystals, in aperiodic and quasi-periodic chains and in random environments [20, 21, 36]. There, the highlighted dramatic deviations from the ballistic behaviour (expected for regular, infinite lattices) range from anomalous to superdiffusion, to decoherence and even to Anderson localization [37].

Here, we consider the case in which non-regularity stems from the intrinsic spatial inhomogeneity of the substrate (for DSGs and CTs) and we also study quantum walks on STs which allow us to evidence the role of finiteness. From the experimental side, the importance of such factors (spatial inhomogeneities and finiteness of the sample) has been increasingly recognized (see e.g. [38]), so that it is of great interest to understand to what extent quantum transport is influenced by them.

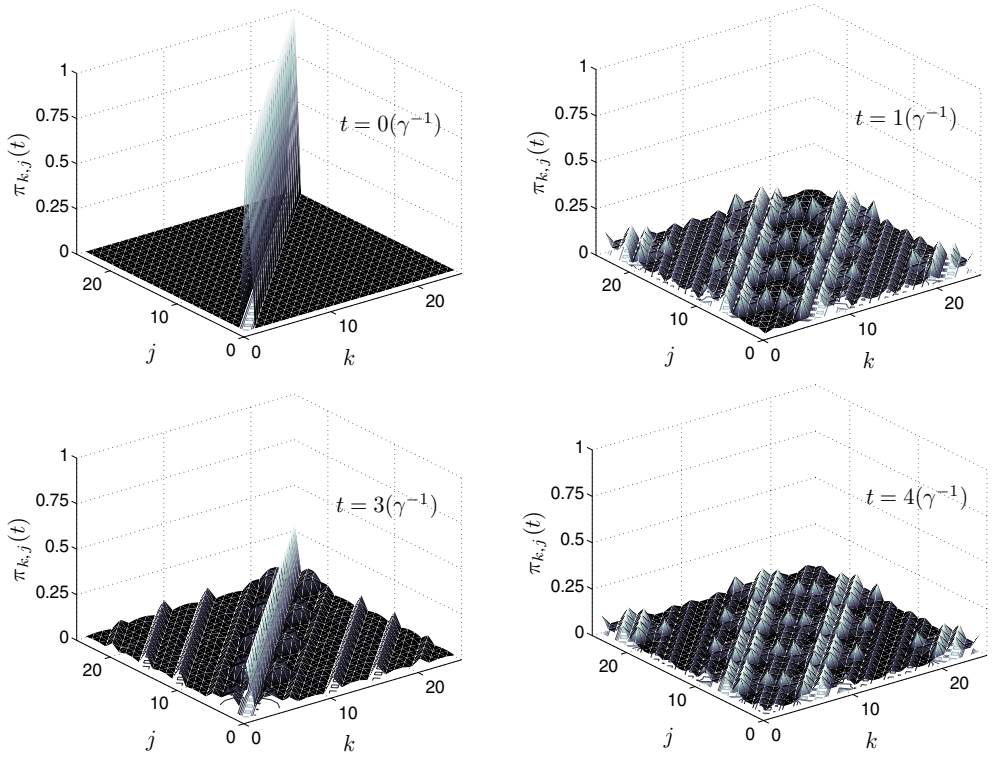

Figure 5. Snapshots of the transition probability $\pi_{k,j}(t)$ at different times $t = 0, 1, 3, 4$ (in units of γ^{-1}) for the square torus of linear size $L = 5(\mathcal{N} = 25)$. Note that the distribution spreads very rapidly and regularly over the whole structure.

First, we note that the fact that $\pi_{k,j}(t)$ does not attain a stationary distribution also causes the average displacement $\langle r_j(t)\rangle_q$ not to necessarily increase monotonically with t. Moreover, due to reflection effects, we expect the mean value $\overline{\langle r(t)\rangle}_q$ to overestimate the displacement performed by a CTQW that started from a peripheral site. Indeed, one finds for the DSG and the CT that $\overline{\langle r(t)\rangle}_q$ is larger than $\langle r_j(t)\rangle_q$, j being any corner of the gasket (see figure 6) or any peripheral site, respectively. As for the ST, $\overline{\langle r(t)\rangle}_q$ trivially equals $\langle r_j(t)\rangle_q$, for all j.

As mentioned above, for classical diffusion the average displacement grows continuously from zero to a maximum value r_c which, due to equipartition, is just the mean distance among sites:

$$r_c = \frac{1}{\mathcal{N}^2}\sum_{k,j=1}^{\mathcal{N}} \ell(k, j). \tag{15}$$

Despite the oscillating behaviour of $\overline{\langle r(t)\rangle}_q$, we can obtain an analogous constant value r_q, around which the average displacement eventually fluctuates, which reads

$$r_q \equiv \lim_{T\to\infty}\frac{1}{T}\int_0^T \mathrm{d}t\,\overline{\langle r(t)\rangle}_q. \tag{16}$$

Otherwise stated, $\overline{\langle r(t)\rangle}_q$ eventually reaches a 'stationary regime' in which it fluctuates around a constant value (see figure 7).

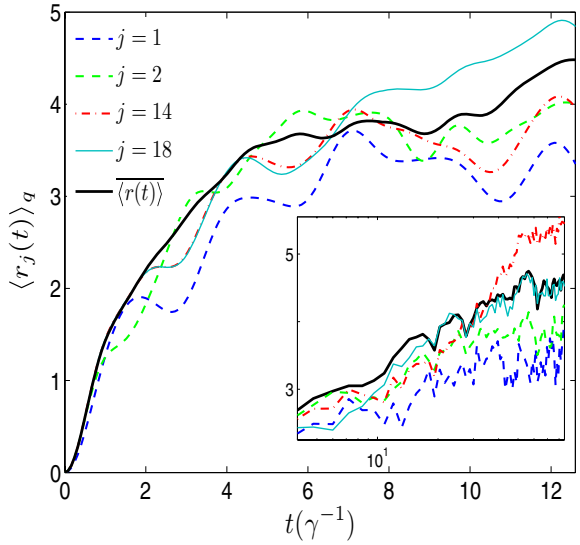

Figure 6. Average displacement $\langle r_j(t)\rangle_q$ for a quantum walker which started at the jth site on a DSG of generation $g = 5$. The main figure focuses on short times, while in the inset a wider temporal range is considered. Different colours and thicknesses distinguish different initial sites j, as shown in the legend; the labelling is the same as in figure 2. Note the appearance of local minima from $t \approx \gamma^{-1}$ onwards.

Of course, r_q and r_c depend on both the topology and the size of the substrate, and they diverge as $\mathcal{N} \to \infty$. From the remarks of section 4.1, we expect that quantum interference arising from reflection affects r_q, making it smaller than r_c. Indeed, for the CT and the DSG, figure 7 clearly shows that $r_q < r_c$; this is especially apparent for the CT where $r_c \approx 8.9$ (calculated from equation (15)) is nearly four times larger than $r_q \approx 2.4$. Conversely, for the ST, where interference only stems from the superposition of waves which have crossed the whole substrate, we find that r_c and r_q are eventually comparable. Therefore, we expect that on structures endowed with reflecting boundaries (i.e. peripheral nodes of low connectivity), at sufficiently long times, the expectation value of the average distance reached by a quantum particle is strictly smaller than the average distance r_c among the nodes.

The classical and the quantum cases are further compared in figure 8 which shows the ratio $\overline{\langle r(t)\rangle}_c / \overline{\langle r(t)\rangle}_q$: one can note that, for significant times ($t > 1\gamma^{-1}$), the classical average displacement is strictly lower than the quantum-mechanical one up to time $t \approx 4\gamma^{-1}$, $t \approx 9\gamma^{-1}$ and $t \approx 18\gamma^{-1}$ for CT, ST and DSG, respectively.

Thus, we can conclude that, on restricted geometries such as those analysed here, CTQWs can spread faster than their classical counterpart, although the advantage is significant only at relatively short times. Moreover, the spatial homogeneity enhances the speed-up; especially for CTs and, in general, for tree-like structures, the large number of peripheral sites gives rise to localization effects which significantly reduce r_q.

Finally, we stress that analytical results on the average displacement performed by a quantum particle on discrete structures are rather sparse (see e.g. [16, 39]); in the appendix we prove that on infinite d-dimensional hypercubic lattices both the average chemical displacement defined in section 2.1 and the Euclidean displacement depend linearly on time and that this kind of behaviour survives, at short times, also for finite lattices.

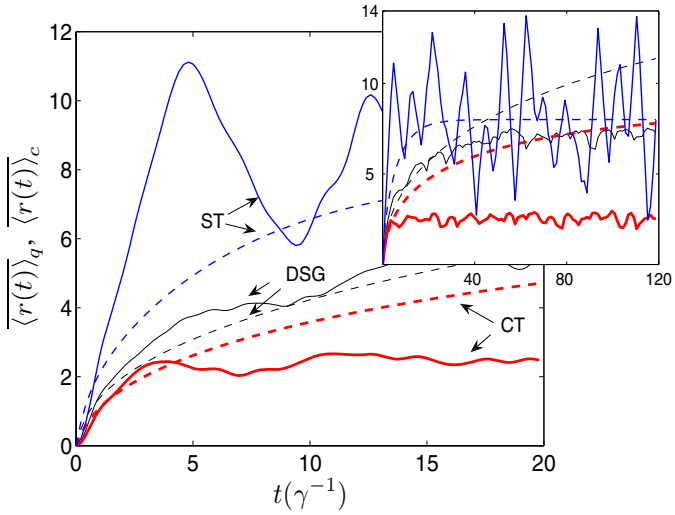

Figure 7. Classical (dashed line) and quantum (continuous line) average displacement for the DSG ($g = 5, \mathcal{N} = 243$), the CT ($g = 6, \mathcal{N} = 190$) and the ST ($L = 16, \mathcal{N} = 256$). The main figure focuses on the short-time regime, while the inset also shows the long-time regime.

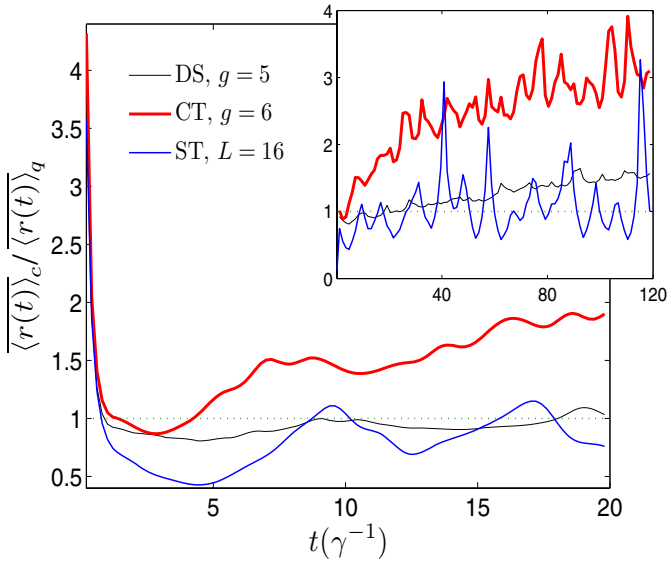

Figure 8. Ratio between classical and quantum average displacement for the DSG ($g = 5$), the CT ($g = 6$) and the ST ($L = 16$), as shown by the legend. The main figure focuses on the short-time, while the inset also shows the long-time regime. In particular, for the square torus, the ratio $\overline{\langle r(t)\rangle_c}/\overline{\langle r(t)\rangle_q}$ is first smaller than unity and then it oscillates around unity; the highest peaks are signs of (partial) revivals.

4.3. Average return probability

The average displacement for CTQWs already highlighted some aspects of the role of inhomogeneities for transport processes. Now, we obtain further insights by considering the average return probability.

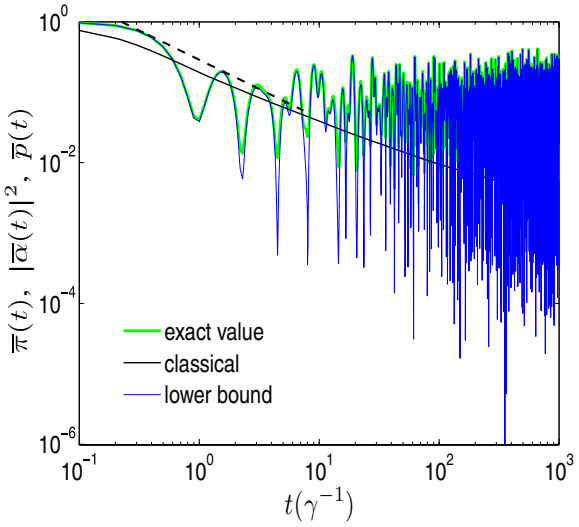

Figure 9. Average return probability $\bar{\pi}(t)$ for the DSG of generation $g = 5$ on a log–log scale. The comparison with the classical $\bar{p}(t)$ evidences that the classical random walk spreads more efficiently than its quantum-mechanical counterpart. The dashed line represents the envelope of $\bar{\pi}(t)$.

For the DSG we can get $\bar{p}(t)$ without numerically diagonalizing $\mathbf{L}$, since it only depends on eigenvalues which can be calculated iteratively. Figure 9 displays the averaged probabilities $\bar{p}(t), \bar{\pi}(t)$ and $|\bar{\alpha}(t)|^2$—numerically evaluated from equations (11), (12) and (13), respectively—as a function of time, obtained for $g = 5$. The classical $\bar{p}(t)$ decays monotonically to the equipartition value $1/\mathcal{N}$, while the quantum-mechanical probabilities eventually oscillate around the value 0.7, which is larger than 3^{-g}. Although the amplitude of fluctuations exhibited by the lower bound is larger than that of the exact value, the agreement between the two quantities is very good. In particular, the positions of the extrema practically coincide and the maxima of $\bar{\pi}(t)$ are well reproduced by the lower bound. An analogous behaviour was also found for other graphs, such as square lattices [13], Cayley trees [31] and stars [29]. Note, however, that for the square lattices the lower bound turns out to be exact while for Cayley trees and for stars it is only an approximation, which, moreover, turns out to be less accurate than what we find here for the DSG.

On short times ($t < 5\gamma^{-1}$) it is possible to construct the envelope of $\bar{\pi}(t)$, which depends algebraically on t. The exponent is ≈ -0.82, to be possibly compared with $\tilde{d}/2 \approx -0.68$ which is the exponent expected classically for the infinite DSG. The decay of the average return probability $\bar{\pi}(t)$ for the ST can be estimated as well: its envelope goes like t^{-2} (classically as $\bar{p}(t) \sim t^{-1}$) [13, 30], implying a faster delocalization of the CTQW over the graph.

Interestingly, for the DSG, the overall shape of $\bar{\pi}(t)$ does not depend significantly on the size of the gasket (figure 10). In fact, the behaviour of $\bar{\pi}(t)$ is mainly controlled by the most highly degenerate eigenvalues. These do not change when increasing the fractal size (i.e. its generation). These values are 3 with degeneracy $m_g(3) = (3^{g-1} + 3)/2$, 5 with degeneracy $m_g(5) = (3^{g-1} - 1)/2$ and $(5 \pm \sqrt{13})/2$ with degeneracy $m_{g-1}(3)$, see section 3.

4.4. Long-time averages

As underlined in section 2, the unitary time evolution does not allow a definite long-time limit for $\pi_{k,j}(t)$. Then, in order to obtain information about the overall spreading of quantum walks,

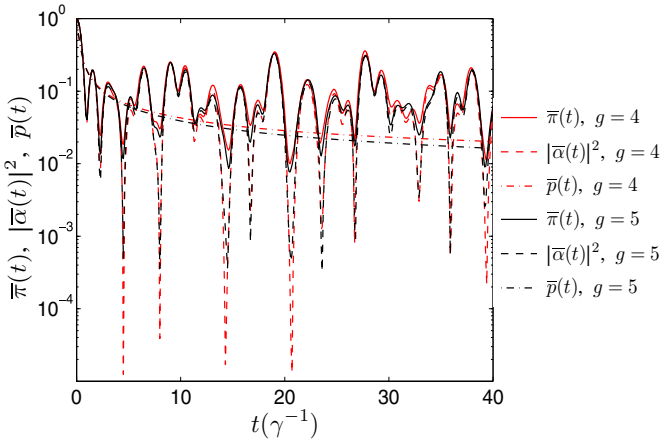

Figure 10. Average return probability $\bar{\pi}(t)$ for the DSG of generation $g = 4$ (bright colour) and $g = 5$ (dark colour). Its lower bound $|\bar{\alpha}(t)|^2$ (dashed line) and the classical $\bar{p}(t)$ (dotted line) are also depicted, as shown by the legend.

it is advantageous to use the long-time average:

$$\chi_{k,j} \equiv \lim_{T\to\infty} \frac{1}{T} \int_0^T \mathrm{d}t\, \pi_{k,j}(t) = \sum_{n,m} \delta_{\lambda_n,\lambda_m} \langle k|\psi_n\rangle\langle\psi_n|j\rangle\langle j|\psi_m\rangle\langle\psi_m|k\rangle, \tag{17}$$

where $\delta_{\lambda_n,\lambda_m}$ equals 1 for $\lambda_n = \lambda_m$ and is zero otherwise. The LTA of $\bar{\pi}(t)$ follows as

$$\bar{\chi} \equiv \lim_{T\to\infty} \frac{1}{T} \int_0^T \mathrm{d}t\, \bar{\pi}(t) = \frac{1}{\mathcal{N}} \sum_{n,m,j} \delta_{\lambda_n,\lambda_m} |\langle j|\psi_n\rangle|^2 |\langle j|\psi_m\rangle|^2, \tag{18}$$

for which we obtain a lower bound which does not depend on the eigenvectors [29]:

$$\bar{\chi} \geqslant \frac{1}{\mathcal{N}^2} \sum_{n,m} \delta_{\lambda_n,\lambda_m} \equiv \bar{\chi}_{\mathrm{lb}}. \tag{19}$$

We first consider the DSG for which figure 11 shows $\chi_{k,j}$ as a contour plot, whose axes are labelled by the nodes $k = 1, \ldots, \mathcal{N}$ and $j = 1, \ldots, \mathcal{N}$. Bright shades correspond to large; dark ones to small LTAs. First, we note that the LTAs are far from being homogeneous and, hence, are not equipartitioned. In particular, the values on the main diagonal are high, meaning that CTQWs have a high LTA probability to be at the starting node.

The inhomogeneity of the pattern mirrors the lack of translation invariance of the DSG itself. For instance, v being the label assigned to any vertex of the main triangle, $\chi_{v,v}$ is a global maximum; off-diagonal local maxima correspond to couples of connected nodes belonging to different minor triangles of generation $g - 1$. This allows us to establish a mapping between the pattern of $\chi_{k,j}$ and the structure of the relevant DSG. Indeed, as suggested by the white delimiting lines in figure 11, the patterns of the LTA distributions exhibit self-similarity.

As for $\bar{\chi}$ and its lower bound $\bar{\chi}_{\mathrm{lb}}$, we recall that the former can be calculated numerically, once all eigenvalues and eigenvectors of the Laplacian operator are known (equation (18)), while for the latter the knowledge of the eigenvalue spectrum is sufficient

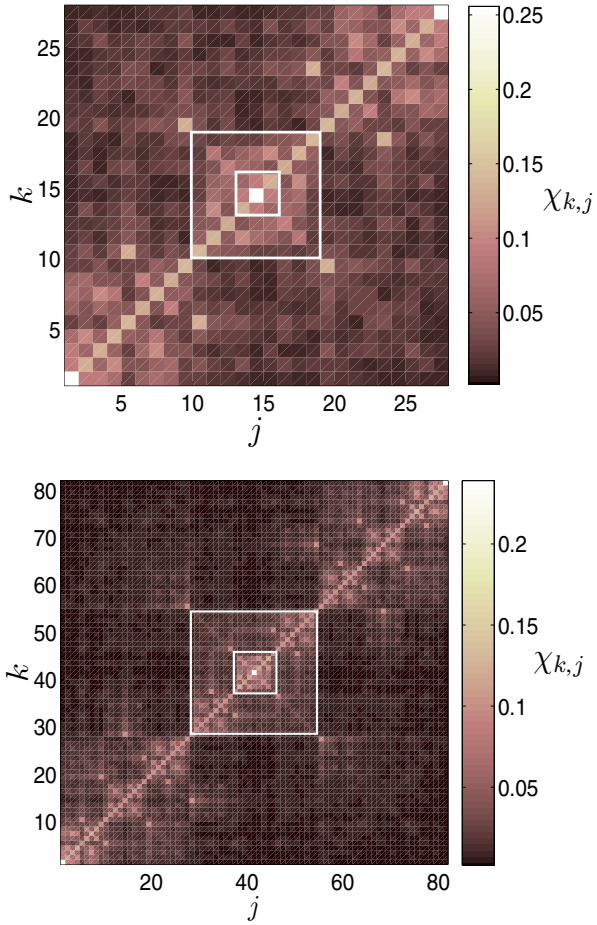

Figure 11. Limiting probabilities for the DSG of generation $g = 3$ (top) and $g = 4$ (bottom), whose volumes are $\mathcal{N} = 27$ and $\mathcal{N} = 81$, respectively. The white delimiting lines enclose the limiting distributions for gaskets of smaller generations. Note that the global maxima lay on the main diagonal and correspond to $j = 1, 14, 27$ and to $j = 1, 41, 81$ for $g = 3$ and for $g = 4$, respectively.

(equation (19)). Since the spectrum of the DSG is known, we can calculate $\bar{\chi}_{\rm lb}$ analytically. Recalling the results of section 3, at generation g the spectrum of $\mathbf{L}$ displays $\tilde{\mathcal{N}}$ distinct eigenvalues, where

$$\tilde{\mathcal{N}} = \sum_{r=0}^{g-1} 2^r + \sum_{r=0}^{g-2} 2^r + 1 = 3 \times 2^{g-1} - 1.$$

We call the set of distinct eigenvalues $\{\tilde{\lambda}_i\}_{i=1,\ldots,\tilde{\mathcal{N}}}$. Being $m(\lambda_i)$ the degeneracy of the eigenvalue λ_i, we can write

$$\mathcal{N}^2 \bar{\chi}_{\rm lb} = \sum_{n,m=1}^{\mathcal{N}} \delta_{\lambda_n,\lambda_m} = \sum_{n=1}^{\mathcal{N}} m(\lambda_n) = \sum_{i=1}^{\tilde{\mathcal{N}}} [m(\tilde{\lambda}_i)]^2.$$

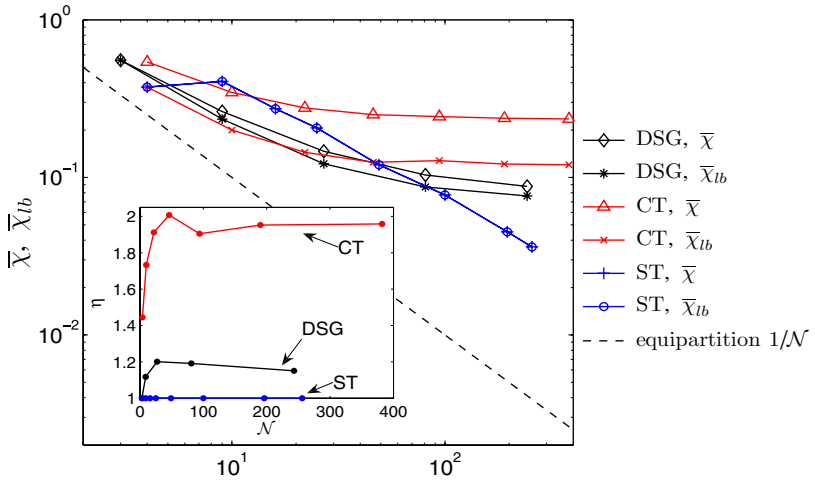

Figure 12. Long-time average $\bar{\chi}$ and its lower bound $\bar{\chi}_{\rm lb}$ calculated according to equation (20) for the dual Sierpinski gasket (diamonds and stars), the Cayley tree (triangles and diagonal crosses) and the square torus (crosses and open circles) versus the size of the structure $\mathcal{N}$; lines are guides for the eye. The dashed line represents the equipartition value $1/\mathcal{N}$. Inset shows the ratio η as a function of $\mathcal{N}$. Note that $\eta(\mathcal{N}) \equiv 1$ holds not only for the periodic square lattice, but for all hypercubic lattices.

Now, we go over to the space of distinct degeneracies, each corresponding to a number ρ of distinct eigenvalues and we get the final, explicit formula

$$\begin{aligned}\bar{\chi} \geqslant \bar{\chi}_{\rm lb} &= \frac{1}{\mathcal{N}^2}\sum_{r=0}^{2g}[m(r)]^2\rho(m(r)) \\ &= \frac{1}{\mathcal{N}^2}\left\{\sum_{r=0}^{g-1}\left[\frac{3^{g-r-1}+3}{2}\right]^2\times 2^r+\sum_{r=0}^{g-2}\left[\frac{3^{g-r-1}-1}{2}\right]^2\times 2^r+1\right\} \\ &= \frac{1}{3^{2g}}\left[3^g\left(1+\frac{3^g}{14}\right)+\frac{10}{7}2^g-\frac{3}{2}\right] > \frac{1}{3^g}. \end{aligned} \tag{20}$$

Interestingly, in the limit $g \to \infty$, the LTA $\bar{\chi}$ is finite:

$$\bar{\chi} \geqslant \lim_{g\to\infty}\bar{\chi}_{\rm lb} = \frac{1}{14}$$

and $\bar{\chi}_{\rm lb}$ reaches this asymptotic value from above.

In figure 12 we show, as functions of $\mathcal{N}$, $\bar{\chi}$ and its lower bound, calculated from equations (18) and (20). For comparison, the same quantities obtained for CTs and STs are also depicted. In the latter case, due to the regularity and periodicity of the lattice [40], the lower bound actually coincides with the exact value. For all cases considered, $\bar{\chi}$ is larger than the equipartition value (given by the dashed line).

The inset of figure 12 shows the ratio

$$\eta(\mathcal{N}) \equiv \frac{\bar{\chi}}{\bar{\chi}_{\rm lb}}.$$

Obviously, the closer η is to 1, the better $\bar{\chi}_{\rm lb}$ approximates $\bar{\chi}$. In this sense, the lower bound calculated for CTs is not as good an approximation to $\bar{\chi}$ as is for the DSG and for the ST. For

the CT, $\bar{\chi}_{\rm lb}$ definitely underestimates, being about half the exact value of $\bar{\chi}$. The quantity $\eta(\mathcal{N})$ may act as a measure of the inhomogeneity of a given substrate. Practically, when dealing with a large sized, sufficiently regular structure, we can get information about the localization of a quantum particle moving on it simply through $\bar{\chi}_{\rm lb}$, thus avoiding the (lengthy) evaluation of the eigenvector set.

5. Conclusions

We investigated the behaviour of continuous-time quantum walks on finite discrete structures characterized by different topologies; we considered the square torus, the Cayley tree and the dual Sierpinski gasket.

The interplay between the quantum-walk dynamics and the underlying topology was deepened by studying, in particular, the temporal evolution of the transfer probability distribution and the ratio $\bar{\chi}/\bar{\chi}_{\rm lb}$ as a function of the substrate size. The latter turns out to be significantly sensitive to the inhomogeneity of the substrate, from which we can infer that lower-bound estimates are especially reliable for regular structures.

From an applied, as well as theoretical, perspective, the average displacement of the walker, as a function of time, also plays an important role. This quantity is not only directly related to the transport properties, but it also provides information about how fast the walk explores the underlying structure, allowing an immediate comparison with the classical case. We found that at short times, CTQWs can spread faster than their classical counterparts, although spatial inhomogeneities and finiteness jointly reduce this effect. In the appendix we prove that for infinite d-dimensional hypercubic lattices, at long times both the average chemical and the Euclidean displacements depend linearly on time (i.e. the motion is ballistic); for finite lattices this kind of behaviour holds at relatively short times only.

Acknowledgments

EA thanks the Italian Foundation 'Angelo della Riccia' for financial support. Support from the Deutsche Forschungsgemeinschaft (DFG), the Fonds der Chemischen Industrie and the Ministry of Science, Research and the Arts of Baden-Württemberg (AZ: 24-7532.23-11-11/1) is gratefully acknowledged.

Appendix A. Average chemical displacement on hypercubic lattices

Here we consider infinite d-dimensional hypercubic lattices and, by exploiting their translational invariance, we prove that on them the average chemical displacements of CTQWs, as defined in section 2.1, depend linearly on time. We first focus on the infinite discrete chain, then we consider the generic d-dimensional case and finally we analyse the two-dimensional lattice.

For a ring of length $\mathcal{N}$, by exploiting the Bloch states, we have [41]

$$\alpha_{k,j}(t) = \frac{1}{\sqrt{\mathcal{N}}} \sum_{l} \mathrm{e}^{-\mathrm{i}\lambda_l t}\, \mathrm{e}^{-\mathrm{i}l(k-j)}, \tag{A.1}$$

where λ_l is the lth eigenvalue of the Laplacian matrix $\mathbf{L}$ associated with the ring. In the limit $\mathcal{N} \to \infty$ we are allowed to replace the sum over l by an integral, obtaining

$$\lim_{\mathcal{N}\to\infty} \alpha_{k,j}(t) = \mathrm{i}^{k-j}\, \mathrm{e}^{-\mathrm{i}2t}\, J_{k-j}(2t), \tag{A.2}$$

where $J_k(z)$ is the Bessel function of the first kind. In the calculation of the transfer probability $\pi_{k,j}(t)$ the phase factor vanishes and we have $\pi_{k,j}(t) = J^2_{k-j}(2t)$, which can be restated as

$$\pi_{k,0}(t) = J^2_k(2t), \tag{A.3}$$

due to the translational invariance of the structure. Clearly (in agreement with $\pi_{k,0}(t)$ being a probability distribution), one has for all t

$$\sum_{k=-\infty}^{+\infty} \pi_{k,0}(t) = \sum_{k=-\infty}^{+\infty} J^2_k(2t) = J^2_0(2t) + 2\sum_{k=1}^{\infty} J^2_k(2t) = 1, \tag{A.4}$$

the last equality being based on $J_k(z) = (-1)^k J_{-k}(z)$ and on equation (8.536.3) in [42].

Now, the average chemical displacement of a CTQW which starts from 0 and moves on an infinite chain (subscript q, 1) follows from equation (5) as

$$\begin{aligned}\langle r_0(t)\rangle_{q,1} = \langle r(t)\rangle_{q,1} &= \sum_{k\in V} \ell(k,0) J^2_k(2t) \\ &= \sum_{k=-\infty}^{\infty} |k| J^2_k(2t) = 2\sum_{k=1}^{\infty} k J^2_k(2t).\end{aligned} \tag{A.5}$$

Here, in the first equality we dropped the subscript 0 due to the equivalence between the sites and in the last equality we exploited the symmetry of the Bessel functions, $J^2_{-k}(z) = J^2_k(z)$. Now, recalling the recursion formula equation (8.471.1) in [42]

$$J_{k-1}(z) + J_{k+1}(z) = \frac{2k}{z} J_k(z), \tag{A.6}$$

we can write

$$2\sum_{k=1}^{\infty} k J^2_k(z) = z\sum_{k=1}^{\infty} [J_{k-1}(z)J_k(z) + J_k(z)J_{k+1}(z)] \equiv z\mathcal{J}(z), \tag{A.7}$$

by defining the function $\mathcal{J}(z)$. Hence

$$\left\langle r_k\left(\frac{z}{2}\right)\right\rangle_{q,1} = z\mathcal{J}(z), \tag{A.8}$$

where we put $2t = z$. The squared Bessel function $J^2_k(z)$ is almost everywhere positive and the analysis of its zeros allows us to state that, for $t > 0$, the sum appearing in the left-hand side of equation (A.8) is strictly positive; the same holds therefore for $\mathcal{J}(z)$, for which we also note from equation (A.7) that $\mathcal{J}(0) = 0$. Moreover, through the following recursion formula, equation (8.471.2) in [42]

$$2\frac{\partial}{\partial z} J_k(z) = J_{k-1}(z) - J_{k+1}(z), \tag{A.9}$$

it follows by directly differentiating $\mathcal{J}(z)$ and rearranging the terms

$$\frac{\mathrm{d}}{\mathrm{d}z}\mathcal{J}(z) = \frac{J_0(z)[J_0(z) + J_2(z)]}{2} = \frac{J_0(z)J_1(z)}{z}, \tag{A.10}$$

where in the last expression we again used equation (A.6) for $k = 1$. The indefinite integral of equation (A.10) is (see equation (5.53) in [42])

$$\mathcal{J}(z) = zJ^2_0(z) + zJ^2_1(z) - J_0(z)J_1(z) + C, \tag{A.11}$$

as can be simply verified by differentiating equation (A.11) and using equations (A.6) and (A.9). Furthermore, since $\mathcal{J}(0) = 0$, we have $C = 0$.

Therefore, the following, for us fundamental, relation holds:

$$\sum_{k=1}^{\infty} k J_k^2(z) = \frac{z}{2}\left[z J_0^2(z) + z J_1^2(z) - J_0(z) J_1(z)\right]. \tag{A.12}$$

Now, from equations (A.5) and (A.12) we get the exact expression for the average chemical displacement

$$\left\langle r\left(\frac{z}{2}\right)\right\rangle_{q,1} = z[z J_0(z)^2 + z J_1(z)^2 - J_0(z) J_1(z)]. \tag{A.13}$$

For large $z = 2t$ (i.e. long times) we can use the expansion (see equation (8.451.1) in [42])

$$J_k(z) = \sqrt{\frac{2}{\pi z}}\left[\cos\left(z - \frac{k\pi}{2} - \frac{\pi}{4}\right) + O\left(\frac{1}{z}\right)\right]. \tag{A.14}$$

Consequently, inserting equation (A.14) for $J_0(z)$ and $J_1(z)$ into (A.13), we infer that the long-time behaviour of the average chemical CTQW displacement on an infinite chain obeys

$$\langle r(t)\rangle_{q,1} \sim \frac{4t}{\pi}. \tag{A.15}$$

This result is consistent with findings reported in [39] for the average square displacement.

Let us now consider higher-dimensional hypercubic lattices. Again, without loss of generality, we can assume the CTQW to start from the point $\mathbf{0} = (0, 0, \ldots, 0)$ so that the chemical distance attained by a walker being at the generic site $\mathbf{k} = (k_1, k_2, \ldots, k_d)$ is $\ell(\mathbf{k}, \mathbf{0}) = |k_1| + |k_2| + \cdots + |k_d|$. Furthermore, on a hypercubic lattice, assuming symmetric conditions in all directions, the probability distribution $\pi_{\mathbf{k},\mathbf{0}}(t)$ factorizes into the d-independent one-dimensional distributions $\pi_{k_j,0}(t)$:

$$\pi_{\mathbf{k},\mathbf{0}}(t) = \pi_{k_1,0}(t)\pi_{k_2,0}(t)\cdots\pi_{k_d,0}(t) = \prod_{j=1}^{d} \pi_{k_j,0}(t). \tag{A.16}$$

Hence

$$\langle r_{\mathbf{0}}(t)\rangle_{q,d} = \left\langle \sum_{j=1}^{d} |k_j| \right\rangle_{q,d} = \sum_{j=1}^{d} \langle |k_j|\rangle_{q,d} = \sum_{j=1}^{d} \langle |k_j|\rangle_{q,1} = d\langle r_0(t)\rangle_{q,1}. \tag{A.17}$$

In the last relation we used the fact that $\langle |k_j|\rangle_{q,d} = \langle |k_j|\rangle_{q,1}$ since for each j only the distribution $\pi_{k_j,0}(t)$ matters, the other distributions adding up to a factor of unity each. Hence

$$\langle r(t)\rangle_{q,d} = d\langle r(t)\rangle_{q,1} \sim \frac{4\,dt}{\pi}. \tag{A.18}$$

In particular, for the square lattice we have

$$\langle r(t)\rangle_{q,2} \sim \frac{8t}{\pi}, \tag{A.19}$$

which was used in figure A1 (dashed line) to fit data relevant to the average chemical displacement performed by a CTQW on square tori of different (finite) sizes. As can be seen from the figure, the ballistic behaviour also holds for finite lattices, but for relatively short times only: at longer times the finiteness of the lattice starts to matter and the product of Bessel functions in equation (A.16) ceases to be a good approximation of the transfer probability. When the waves associated with CTQWs have crossed the whole lattice, interference effects start to occur and $\langle r(t)\rangle_{q,2}$ exhibits a non-monotonic behaviour. From the same figure we also note that the $O(1/t)$ contributions of equation (A.14) get to be negligible for $t > 1\gamma^{-1}$.

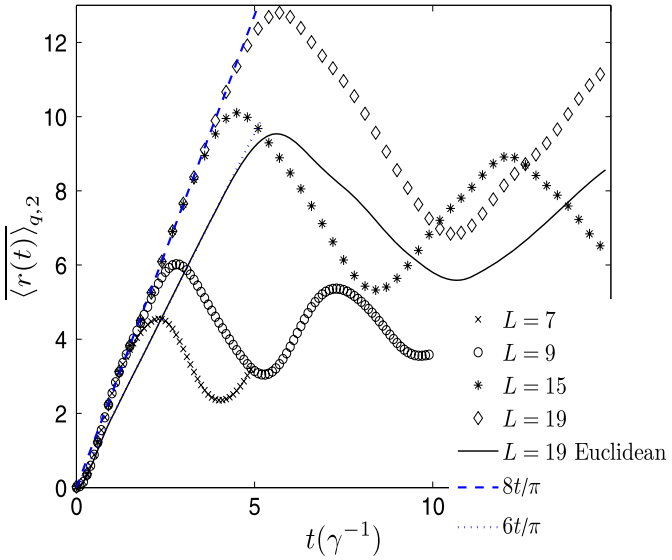

Figure A1. Average chemical displacement $\overline{\langle r(t)\rangle}_q$ for the torus, calculated according to equation (6) (symbols); the line represents the Euclidean average displacement for $L = 19$. The dotted and the dashed lines highlight the linear dependence on t exhibited by the average chemical distance and by the average Euclidean distance, respectively.

In figure A1 we also show data for the average Euclidean displacement which displays a ballistic behaviour at short times as well. Indeed, for a hypercubic lattice of arbitrary dimension d, the following relation holds (see e.g. [43]):

$$\tfrac{1}{\sqrt{3}}\ell(\mathbf{k},\mathbf{j}) \leqslant \|\mathbf{k}-\mathbf{j}\| \leqslant \ell(\mathbf{k},\mathbf{j}), \tag{A.20}$$

where $\|\mathbf{k}-\mathbf{j}\|$ denotes the Euclidean distance between the lattice points $\mathbf{k}$ and $\mathbf{j}$ chosen arbitrarily. By averaging each term of the previous equation with respect to the transfer probability $\pi_{\mathbf{k},\mathbf{j}}(t)$ (we can again exploit the translational invariance of the substrate and fix $\mathbf{j} = \mathbf{0}$), we find that the average Euclidean distance also scales linearly with time with a multiplicative factor bounded between $4d/(\sqrt{3}\pi) \approx 2.31d/\pi$ and $4d/\pi$. In particular, for the square torus of size $L = 19$ considered in figure A1, we find that at relatively short times the average Euclidean distance scales as $6t/\pi$.

References

[1] Kempe J 2003 *Contemp. Phys.* **44** 307
[2] Sanders B C, Bartlett S D, Tregenna B and Knight P L 2003 *Phys. Rev.* A **67** 042305
[3] Lahini Y, Avidan A, Pozzi F, Sorel M, Morandotti R, Christodoulides D N and Silberberg Y 2008 *Phys. Rev. Lett.* **100** 013906
[4] Dür W, Raussendorf R, Kendon V M and Briegel H-J 2002 *Phys. Rev.* A **66** 052319
[5] Côté R, Russell A, Eyler E E and Gould P L 2006 *New J. Phys.* **8** 156
[6] Zou X, Dong Y and Guo G 2006 *New J. Phys.* **8** 81
[7] Ryan C A, Laforest M, Boileau J C and Laflamme R 2005 *Phys. Rev.* A **72** 062317
[8] Mülken O, Blumen A, Amthor T, Giese C, Reetz-Lamour M and Weidemüller M 2007 *Phys. Rev. Lett.* **99** 090601
[9] Aharonov Y, Davidovich L and Zagury N 1993 *Phys. Rev.* A **48** 1687
[10] Farhi E and Gutmann S 1998 *Phys. Rev.* A **58** 915

[11] Strauch F W 2006 *Phys. Rev.* A **74** 030301
[12] Štefaňák M, Jex I and Kiss T 2008 *Phys. Rev. Lett.* **100** 020501
[13] Volta A, Mülken O and Blumen A 2006 *J. Phys. A: Math. Gen.* **39** 14997
[14] Mülken O, Pernice V and Blumen A 2007 *Phys. Rev.* E **76** 051125
[15] ben-Avraham D and Havlin S 2001 *Diffusion and Reactions in Fractals and Disordered Systems* (Cambridge: Cambridge University Press)
[16] Vidal J, Mosseri R and Bellissard J 1999 *J. Phys. A: Math. Gen.* **32** 2361
[17] Williams C P 2001 *Comput. Sci. Eng.* **3** 44
[18] Ambainis A 2004 *SIGACT News* **35** 22
[19] Magniez F, Nayak A, Roland J and Santha M 2007 *Proc. ACM Symp. on Theory of Computation (STOC'07)* (New York: ACM) p 575
[20] Yin Y, Katsanos D E and Evangelou S N 2008 *Phys. Rev.* A **77** 022302
[21] Yuan H Q, Grimm U, Repetowicz P and Schreiber M 2000 *Phys. Rev.* B **62** 15569
[22] Alavi Y, Chartrand G, Oellermann O R and Schwenk A J (ed) *Graph Theory, Combinatorics, and Applications* vol 2 (NewYork: Wiley)
[23] Di Vincenzo D P 1995 *Science* **270** 255
[24] Childs A M and Goldstone J 2004 *Phys. Rev.* A **70** 022314
[25] Mülken O, Volta A and Blumen A 2005 *Phys. Rev.* A **72** 042334
[26] Weiss G H 1994 *Aspects and Applications of the Random Walk* (Amsterdam: North-Holland)
[27] Aharonov D, Ambainis A, Kempe J and Vazirani U 2001 *Proc. ACM Symp. on Theory of Computation (STOC'01)* (New York: ACM) p 50
[28] Aarão Reis F D A 1995 *J. Phys. A: Math. Gen.* **28** 6277
[29] Mülken O 2007 arXiv:0710.3453
[30] Mülken O and Blumen A 2006 *Phys. Rev.* E **73** 066117
[31] Mülken O, Bierbaum V and Blumen A 2006 *J. Chem. Phys.* **124** 124905
[32] Konno N 2006 *Quantum Probab. Relat. Top.* **9** 287
[33] Konno N 2006 *Int. J. Quantum Inf.* **4** 1023
[34] Cosenza M G and Kapral R 1992 *Phys. Rev.* A **46** 1850
[35] Blumen A and Jurjiu A 2002 *J. Chem. Phys.* **116** 2636
[36] Cerovski V Z, Schreiber M and Grimm U 2005 *Phys. Rev.* B **72** 054203
[37] Anderson PW 1958 *Phys. Rev.* **109** 1492
[38] Monastyrsky M I 2006 *Topology in Condensed Matter (Springer Series in Solid-State Sciences)* (Berlin: Springer)
[39] Katsanos D E, Evangelou S N and Xiong S J 1995 *Phys. Rev.* B **51** 895
[40] Blumen A, Bierbaum V and Mülken O 2006 *Physica* A **371** 10
[41] Mülken O and Blumen A 2005 *Phys. Rev.* E **71** 036128
[42] Gradshteyn I S and Ryzhik I M 1965 *Table of Integrals, Series and Products* (NewYork: Academic)
[43] Searcóid M O 2007 *Metric Spaces* (London: Springer)